Journal of ELECTRONIC MATERIALS, Vol. 41, No. 6, 2012
DOI: 10.1007/s11664-011-1790-y

Electrochemical Deposition and Characterization of Thermoelectric Ternary $(Bi_xSb_{1-x})_2Te_3$ and $Bi_2(Te_{1-y}Se_y)_3$ Thin Films

YI MA,[1,2] WARUNA WIJESEKARA,[1] and ANDERS E. C. PALMQVIST[1,3]

1.—Department of Chemical and Biological Engineering, Chalmers University of Technology, SE 41296 Gothenburg, Sweden. 2.—e-mail: yma@chalmers.se. 3.—adde@chalmers.se

Thermoelectric thin films of the ternary compounds $(Bi_xSb_{1-x})_2Te_3$ and $Bi_2(Te_{1-y}Se_y)_3$ were synthesized using potentiostatic electrochemical deposition on gold-coated silicon substrates from aqueous acidic solutions at room temperature. The surface morphology, elemental composition, and crystal structure of the deposited films were studied and correlated with preparation conditions. The thermoelectric properties of $(Bi_xSb_{1-x})_2Te_3$ and $Bi_2(Te_{1-y}Se_y)_3$ films, i.e., Seebeck coefficient and electrical resistivity, were measured after transferring the films to a nonconductive epoxy support. $(Bi_xSb_{1-x})_2Te_3$ thin films showed *p*-type semiconductivity, and the highest power factor was obtained for film deposited at a relatively large negative potential with composition close to $Bi_{0.5}Sb_{1.5}Te_3$. In addition, $Bi_2(Te_{1-y}Se_y)_3$ thin films showed *n*-type semiconductivity, and the highest power factor was obtained for film deposited at a relatively small negative potential, having composition close to $Bi_2Te_{2.7}Se_{0.3}$. In contrast to $Bi_2Te_{2.7}Se_{0.3}$ thin films, an annealing treatment was required for $Bi_{0.5}Sb_{1.5}Te_3$ thin films to achieve the same magnitude of power factor as $Bi_2Te_{2.7}Se_{0.3}$. Therefore, $Bi_2Te_{2.7}Se_{0.3}$ thin films appear to be good candidates for multilayer preparation using electrochemical deposition, but the morphology of the films must be further improved.

Key words: Thermoelectric, thin films, $(Bi_xSb_{1-x})_2Te_3$, $Bi_2(Te_{1-y}Se_y)_3$, characterization

INTRODUCTION

Bismuth telluride (Bi_2Te_3)-based compounds are conventional room-temperature thermoelectric materials for a variety of thermoelectric applications.[1] For instance, they can be used in large devices such as thermoelectric generators or in devices with restricted size such as thermal sensors and spot coolers.[2] Thus, a number of different synthesis methods have been developed for Bi_2Te_3-based compounds depending on the shape and quantity required by the target application. Direct crystallization, such as Czochralski, zone melting, and Bridgman method, allows production of high-quality single crystals in bulk form,[3,4] and powder sintering methods offer large-scale manufacturing of oriented polycrystalline bulk materials,[5] while sputtering and evaporation methods are used to fabricate thin-film counterparts for thermoelectric microdevices.[6–8] However, most of these methods involve expensive equipment and complicated preparation processes. Electrochemical deposition has nowadays been recognized as a promising alternative method to synthesize thermoelectric thin films and nanowires.[9,10] Its main advantages include low cost, low temperature and pressure of operation, large deposition area, and high growth rate. In addition, another appealing convenience of electrochemical deposition is that the level of doping and the crystalline state of the deposited material can be controlled by adjusting the operation parameters of the electrochemical deposition, such as electrolyte type and concentration, deposition potential, deposition temperature, etc.

(Received July 11, 2011; accepted September 26, 2011; published online October 13, 2011)

During the past decades, several studies have been devoted to electrochemical preparation of thin films of Bi_2Te_3 and Sb_2Te_3 binary compounds.[11–16] The *p*-type $Bi_{0.5}Sb_{1.5}Te_3$[17–19] and *n*-type $Bi_2Te_{2.7}Se_{0.3}$[20–22] ternary compounds have also attracted attention recently due to the fact that they are found to be the most efficient thermoelectric materials in bulk form for room-temperature applications. However, there are only few research studies that correlate the synthesis conditions and microstructure of electrodeposited thin-film compounds with their thermoelectric properties. This is largely because the necessary use of conducting substrates for electrodeposition interferes with measurement of thin-film transport properties.

In our previous work, a lift-off procedure used to transfer electrodeposited films from conducting substrates to nonconducting epoxy support was devised for measurements of thermoelectric properties, and the thermoelectric characteristics of Bi_2Te_3 and Sb_2Te_3 thin films were reported, respectively.[23,24] We also demonstrated the feasibility of using the electrochemical deposition method to prepare Bi_2Te_3/Sb_2Te_3 multilayers.[23] Preparation of such multilayers is conventionally done by metal-organic chemical vapor deposition (MOCVD).[6] The interest in multilayer structures originates from the theory that the interfaces between heterogeneous layers would scatter phonons more efficiently than electrons and consequently reduce the thermal conductivity while not disturbing electron transport as much. For such materials it is essential that the majority charge carriers are of the same type in each layer. However, this was not the case in our previous multilayer study where we showed that electrodeposited Bi_2Te_3 films were *n*-type semiconductors while Sb_2Te_3 films were *p*-type independent of the elemental composition of the films prepared for the electrodeposition conditions studied.[23] Thus, it is of particular interest to develop *n*-type thin-film alternatives suitable for electrochemical preparation of Bi_2Te_3-based multilayers and *p*-type alternatives suitable for Sb_2Te_3-based multilayers.

In the current paper, we report the electrochemical preparation and thermoelectric characteristics of thin films of *p*-type $(Bi_xSb_{1-x})_2Te_3$ and *n*-type $Bi_2(Te_{1-y}Se_y)_3$ ternary compounds. The electrochemical deposition processes of Bi-Sb-Te and Bi-Te-Se ternary systems on gold-coated silicon substrates are investigated, using cyclic voltammetry. A number of deposition parameters are explored and linked to the surface morphology, crystal structure, and elemental composition of the deposited films. Their in-plane thermoelectric properties, such as electrical resistivity and Seebeck coefficient, were measured at room temperature after transferring the deposited films to an insulating epoxy support.

EXPERIMENTAL PROCEDURES

The electrolyte solutions used in the electrochemical deposition studies were prepared by dissolving $Bi(NO_3)_3{\cdot}5H_2O$, TeO_2, $SbCl_3$ and Na_2SeO_3 (analytical grade, Aldrich-Sigma) in 1 M HNO_3 (70%, Fluka). To completely dissolve $SbCl_3$, 0.67 M tartaric acid (Aldrich-Sigma) was used as a complexing agent for solutions containing antimony, where the more stable $[Sb_2(C_4H_4O_6)_2]^{2+}$ ions were therefore formed. All electrolyte solutions were prepared with MilliQ water (18 MΩ cm) collected from a Barnstead E-pure filtration system, and deaerated by nitrogen gas for 10 min prior to each electrochemical experiment.

Electrochemical deposition of thin films was carried out in nonstirred solutions using a conventional three-electrode polytetrafluoroethylene (PTFE) reaction cell at room temperature. Gold-coated silicon wafers were used as working electrode, placed at the bottom of the cell and sealed with an O-ring. The working electrode was prepared by sputtering (FHR MS150; Anlagenbau GmbH) a 10-nm-thick titanium film onto a silicon wafer [antimony-doped *n*-Si(111) with resistivity < 0.02 Ω cm; Silicon Quest International, Inc.] followed by a 50-nm-thick gold layer. Opposite to the working electrode, a platinum mesh (Alfa) was used as counter electrode, while a Ag/AgCl electrode filled with 3 M KCl electrolyte [Metrohm, 211.5 mV versus normal hydrogen electrode (NHE) at 20°C] was used as reference electrode, to which all potentials in this paper are referred. All electrodes were connected to a computer-controlled potentiostat (Reference 600; Gamry). $(Bi_xSb_{1-x})_2Te_3$ and $Bi_2(Te_{1-y}Se_y)_3$ thin films were prepared by a continuous deposition method where the applied potential was kept constant during a desired period of time to control the film thickness.

The thickness of the deposited films was calculated from the charge transferred during the electrodeposition using the Faraday equation, assuming 100% current efficiency. The thickness of all the films was controlled to be less than 0.6 μm to reduce problems with crack and pinhole formation resulting from the mass transfer limitation of potentiostatic deposition. The calculated thickness was verified by a surface profiler (Tencor P15), which showed that the difference between the calculated thickness and the profiler measurement was less than 5%. The surface morphology of the deposited films was investigated using scanning electron microscopy (SEM, Leo Ultra 55 FEG). The elemental composition of the films was obtained using the SEM combined with energy-dispersive x-ray spectroscopy (EDX) to calculate the average value of the atomic composition at several different places of the films. Phase identification was performed using an x-ray diffractometer (XRD, Siemens D5000) equipped with a standard scintillation detector with Cu K_α radiation (λ = 1.542 Å, 45 kV, 40 mA, step size 0.04°, 2 s/step, sample rotation 60 rpm). To obtain reliable results for the characterization of thermoelectric properties, all the deposited films were transferred from gold-coated silicon substrates to an insulating epoxy support using a methodology

described previously.[24] The electrical resistivity (ρ) and Seebeck coefficient (α) of the transferred films were measured along the in-plane direction of the films at room temperature using a ZEM-3 instrument (ULVAC-RIKO, Inc.). The instrumental error is within 7%. For the Seebeck measurements, the temperature gradient between the two Pt electrodes was controlled within the order of 10 K, 20 K, and 30 K. To reduce the electrical resistivity of $(Bi_xSb_{1-x})_2Te_3$ films to a level measurable by the ZEM-3 instrument, annealing of the films was performed at 130°C for 2 h in an argon atmosphere.

RESULTS AND DISCUSSION

Electrodeposition and Characterization of $(Bi_xSb_{1-x})_2Te_3$ Thin Films

Voltammetric Studies of the Bi-Sb-Te System

The electrochemical behavior of the Bi-Sb-Te ternary system in an acidic solution was analyzed using cyclic voltammetry (CV). As shown in Fig. 1, there is a major reductive peak spanning from 0.05 V to −0.4 V, reaching a maximum at the position labeled C, ca. −0.13 V. Three shoulders labeled A, B, and D are associated with the major peak, indicating that different deposition steps take place during the cathodic scan.[17] According to previous studies, $HTeO_2^+$ ions in an aqueous solution strongly absorb onto gold surfaces.[25,26] Therefore, shoulder A likely corresponds to reduction of $HTeO_2^+$ to Te^0, followed by sequential reduction of Bi^{3+} and Sb^{3+} with Te^0 to form $(Bi_xSb_{1-x})_2Te_3$. The overall reductive reaction pertaining to the cathodic scan can therefore be expressed as two successive reactions:

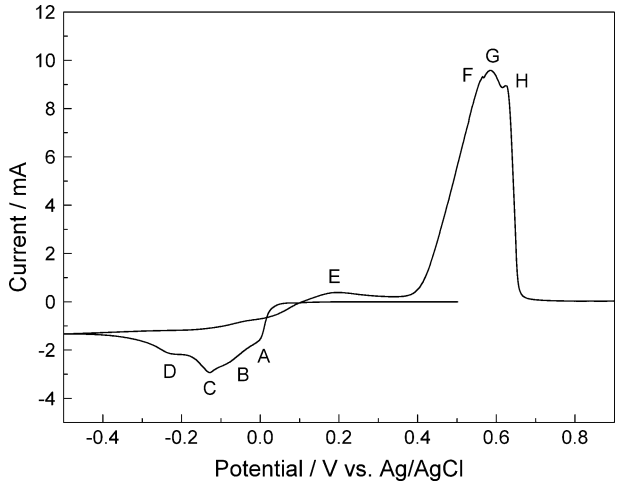

Fig. 1. Cyclic voltammogram of a 1 M HNO_3 solution containing 1.5 mM Bi^{3+}, 3.0 mM $[Sb_2(C_4H_4O_6)_2]^{2+}$, 10.0 mM $HTeO_2^+$, and 0.67 M tartaric acid. The scan starts at the open-circuit potential and proceeds to −0.5 V and is then reversed and swept to 0.9 V using a sweep rate of 10 mV/s. The working electrode is a gold-coated silicon substrate with active area of 0.95 cm^2.

$$HTeO_2^+ + 3H^+ + 4e^- \rightleftharpoons Te^0 + 2H_2O$$

$$3Te^0 + 2(1-x)Bi^{3+} + x[Sb_2(C_4H_4O_6)_2]^{2+} + 6e^- \rightleftharpoons (Bi_{1-x}Sb_x)_2Te_3 + 2x(C_4H_4O_6)^{2-}$$

During the anodic scan, one oxidation wave labeled E and one pronounced oxidation peak labeled G associated with shoulders F and H were observed. Peak E corresponds to oxidation of a bismuth-rich phase of the film, while elemental antimony is also oxidized in this region. Peaks F, G, and H correspond to oxidation of $(Bi_xSb_{1-x})_2Te_3$ compounds.[27] The occurrence of multiple oxidation peaks indicates that the deposits formed during the cathodic scan were not in a single phase. It is, thus, of great interest to characterize the deposits that were formed at the different cathodic potentials. For this, films C1, C2, C3, and C4 were deposited at different constant potentials, E_p, of −0.01 V, −0.08 V, −0.13 V, and −0.23 V, respectively, corresponding to positions A, B, C, and D in the CV curve.

Compositional and Structural Analysis of $(Bi_xSb_{1-x})_2Te_3$ Films

Table I shows the relation between the applied deposition potential and the elemental composition of the resulting films. Interestingly, there are only two elements (Bi and Te) in film C1, which was deposited at −0.01 V, and its molar composition is close to Bi:Te = 1:6. From the XRD analysis of the film shown in Fig. 2, it is clear that it contains two crystalline forms, Bi_3Te_4 and Te. Apparently, electrodeposition of the Bi-Sb-Te ternary system at a relatively small negative potential is dominated by deposition of tellurium, which confirms the previous suggestion that reduction of $HTeO_2^+$ to Te^0 may occur at an early stage of the cathodic scan.

By further increasing the negative deposition potential, the antimony content in the films could be increased as shown for films C2–C4 in Table I. The need for a more negative potential is due to the fact that the reduction potential of the $[Sb_2(C_4H_4O_6)_2]^{2+}$ complex in the solution is much more negative than that of either the bismuth and tellurium ions.[23] Therefore, films C3 and C4 deposited at more negative potentials showed composition much closer to the target composition of $Bi_{0.5}Sb_{1.5}Te_3$. Both films showed XRD patterns that match the standard pattern of polycrystalline $Bi_{0.5}Sb_{1.5}Te_3$ (PDF 04-002-0106), as displayed in Fig. 2. The diffraction peaks of films C3 and C4 appear broader than those of film C1, although the thickness of those films is similar. This suggests that films C3 and C4 may have smaller crystallite sizes than film C1. It is also worth noting that film C2 deposited at a relatively less negative potential compared with films C3 and C4 shows an amorphous structure, which has not been reported previously according to the authors' knowledge.

Table I. Effects of deposition potential and annealing on the elemental composition (atomic percentage) of the prepared film

		As-Deposited (at.%)				Annealed (at.%)			
Sample	**E_p (V)**	**Bi**	**Sb**	**Te**	**Formula**	**Bi**	**Sb**	**Te**	**Formula**
C1	−0.01	13.6	n/a	86.4	$Bi_{0.7}Te_{4.3}$	15.6	n/a	84.4	$Bi_{0.8}Te_{4.2}$
C2	−0.08	10.2	19.2	70.6	$Bi_{0.5}SbTe_{3.5}$	12.2	4.6	83.2	$Bi_{0.5}Sb_{0.2}Te_{3.3}$
C3	−0.13	8.0	26.8	65.2	$Bi_{0.4}Sb_{1.3}Te_{3.3}$	7.6	27.8	64.6	$Bi_{0.4}Sb_{1.4}Te_{3.2}$
C4	−0.23	7.6	25.6	66.8	$Bi_{0.4}Sb_{1.3}Te_{3.3}$	8.4	25.2	66.4	$Bi_{0.4}Sb_{1.3}Te_{3.3}$

All films were deposited at constant potentials, E_p

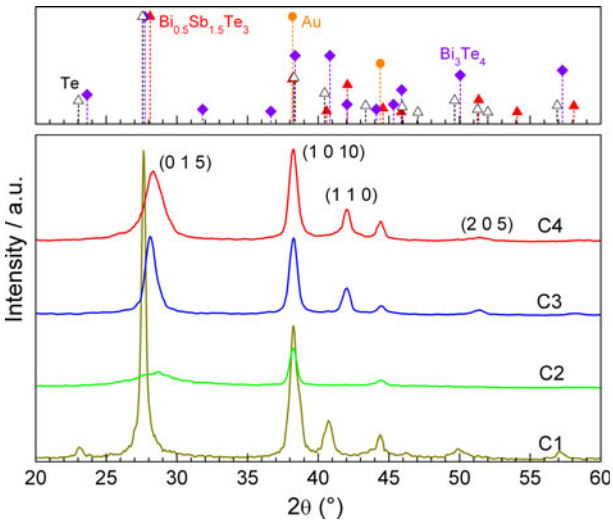

Fig. 2. XRD patterns of as-deposited $(Bi_xSb_{1-x})_2Te_3$ films prepared at different deposition potentials described in Table I. Standard diffraction patterns of gold (dots), tellurium (hollow triangles), Bi_3Te_4 (diamonds), and $Bi_{0.5}Sb_{1.5}Te_3$ (solid triangles) are shown on top.

Noticeable changes in film composition were observed after subjecting the films to an annealing process of 130°C for 2 h in argon atmosphere. The compositional change of film C2 was larger than that of films C1, C3, and C4. Film C2 showed a significant decrease in its antimony content, which was accompanied by a crystallization process during the annealing. This suggests that the compositional change during the annealing is due to selective sublimation of elements that are not bonded stoichiometrically.

Figure 3 shows the surface morphology of as-deposited films C1–C4. Film C1 exhibits a smooth surface with some spherical crystal agglomerates distributed across the surface. The surface of film C2 is characterized by similar spherical crystal agglomerates, but they are more densely packed and slightly smaller in size. Film C3 shows a dendrite-shape morphology, while film C4 shows a cauliflower-shape morphology. These observations indicate that the morphology of the film strongly depends upon the deposition potential, since the potential affects the depletion rate of surface ions as well as the film composition and crystal structure. The morphology of the annealed films (not shown) did not exhibit any obvious difference compared with the as-deposited films, in agreement with our previous observation of electrodeposited Bi_2Te_3 and Sb_2Te_3 films.[23]

Thermoelectric Properties of $(Bi_xSb_{1-x})_2Te_3$ Thin Films

The in-plane electrical resistivity and Seebeck coefficient of the as-deposited and annealed $(Bi_xSb_{1-x})_2Te_3$ films transferred to an insulting epoxy support were measured at room temperature using a ZEM-3 instrument. As shown in Figs. 4a, b, films C1, C3, and C4 have positive Seebeck coefficients for both as-deposited and annealed films, establishing that the films are all *p*-type semiconductors. It was not possible to measure the properties of the as-deposited film C2, presumably due to its amorphous structure having too large an electrical resistivity. Crystallization took place in film C2 during annealing and reduced the electrical resistivity to a level measurable by the ZEM-3 instrument. As shown in Table I, the annealed films C1 and C2 contained a limited amount of antimony and their compositions deviated considerably from the target composition of $Bi_{0.5}Sb_{1.5}Te_3$. Therefore, films C1 and C2 are not as interesting as films C3 and C4 for application as *p*-type multilayer components along with Sb_2Te_3. The positive effect of annealing on decreasing the electrical resistivity was accompanied by an increase in Seebeck coefficient for films C3 and C4, but the magnitude of the change is different, likely due to differences in internal structure, e.g., grain size, shapes, and boundaries. Apparently, film C3 gains the most by annealing in terms of the change in power factor, which includes both the effect of the electric resistivity and the Seebeck coefficient, as shown in Fig. 4b. From this part of the study it was concluded that *p*-type $(Bi_xSb_{1-x})_2Te_3$ thin films with optimal power factor can be deposited at relatively large negative potential, but it is possible that rough surface morphologies may limit the application of electrochemical preparation of multilayers.

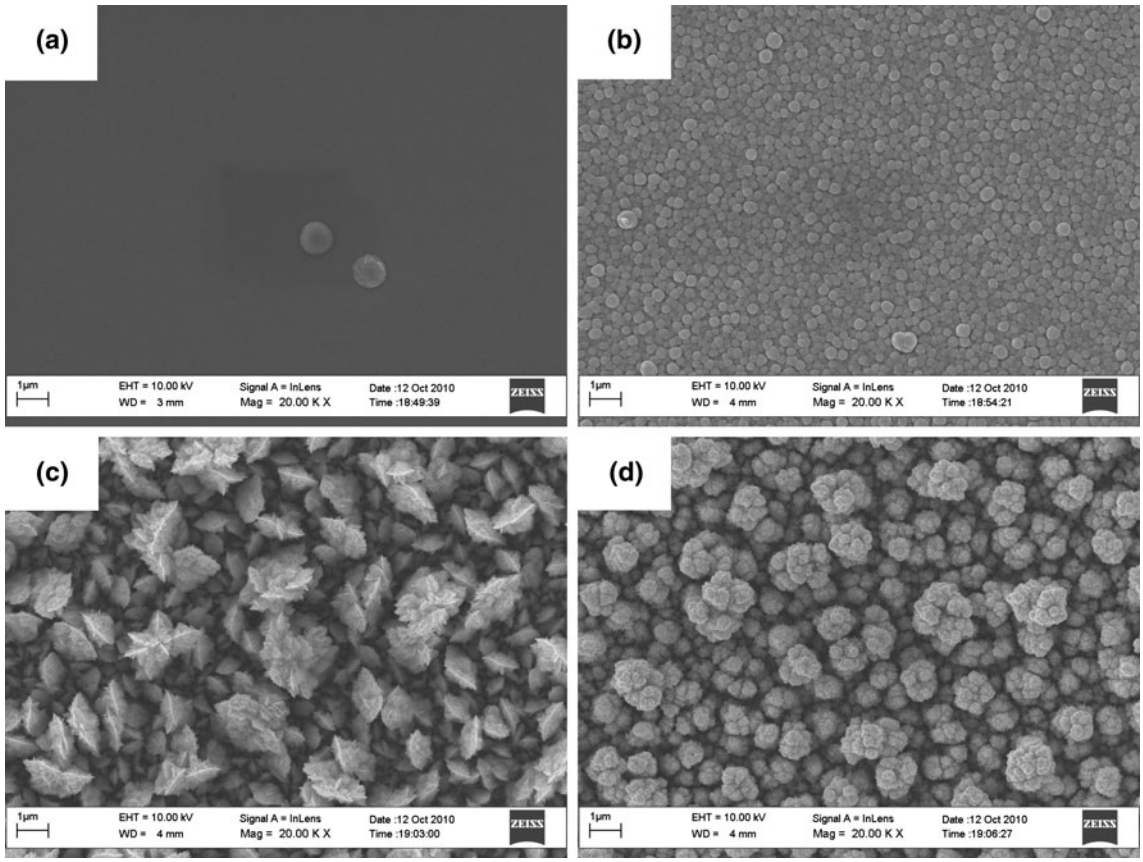

Fig. 3. SEM images of as-deposited $(Bi_xSb_{1-x})_2Te_3$ films (a) C1, (b) C2, (c) C3, and (d) C4.

Electrodeposition and Characterization of $Bi_2(Te_{1-y}Se_y)_3$ Thin Films

Voltammetric Studies of the Bi-Te-Se System

Similar to the Bi-Sb-Te ternary system, the electrochemical behavior of the Bi-Se-Te system was also studied using cyclic voltammetry. As shown in Fig. 5, two consecutive reduction peaks B and C can be observed at ca. 0.045 V and −0.01 V, respectively, indicating two deposition processes for $Bi_2(Te_{1-y}Se_y)_3$, in agreement with the studies by Martin-Gonzalez et al.[28] Due to the presence of SeO_3^{2-}, the reduction peak potential of the ternary system appears more positive than that of Bi_2Te_3 reported previously.[23] This is because the standard reduction potential of SeO_3^{2-}/Se^0 is much more positive than that of Bi^{3+}/Bi^0.[29] As a result of the adsorption of $HTeO_2^+$ on the gold surface, the first reduction peak B can therefore be expected as the deposition of $Te_{1-y}Se_y$ alloy rather than elemental tellurium or selenium. In contrast to published literature,[21] we did not observe the reported color change of the deposits (from pink to black) during the cathodic scan, interpreted as the reduction of Se^0 and subsequent formation of the ternary compound $Bi_2(Te_{1-y}Se_y)_3$. Thus, the overall reaction accompanying the cathodic scan observed here can be described as two consecutive reactions:

$$(1-y)HTeO_2^+ + ySeO_3^{2-} + (3+3y)H^+ + 4e^- \rightleftharpoons Se_{1-y}Te_y + (2+y)H_2O$$

$$2Bi^{3+} + 3Se_{1-y}Te_y + 6e^- \rightleftharpoons Bi_2(Se_{1-y}Te_y)_3$$

Compositional and Structural Analysis of $Bi_2(Te_{1-y}Se_y)_3$ Films

To investigate the dependence of the deposition potential on the morphology, elemental composition, and crystal structure of the electrodeposited $Bi_2(Te_{1-y}Se_y)_3$ films, four different potentials positioned at labels A, B, C, and D along the two reduction peaks in the CV diagram shown in Fig. 5 were chosen to prepare the different films. Table II presents the deposition conditions and the corresponding elemental composition of the deposited films. It can be seen that film E1 deposited at potential A contains relatively high selenium content but low bismuth content compared with the other three films. This is attributed to the fact mentioned previously that the deposition of Se occurs at a more positive potential compared with Bi, and that a $Te_{1-y}Se_y$ alloy may be formed prior to the formation of $Bi_2(Te_{1-y}Se_y)_3$ compounds. Once the deposition potential applied became more negative,

as illustrated by film E2, the selenium content decreased while the bismuth content increased. However, by further decreasing the potential, only minor changes in the elemental composition of the films were observed, especially when compared with the changes for the electrodeposited $(Bi_xSb_{1-x})_2Te_3$ films.

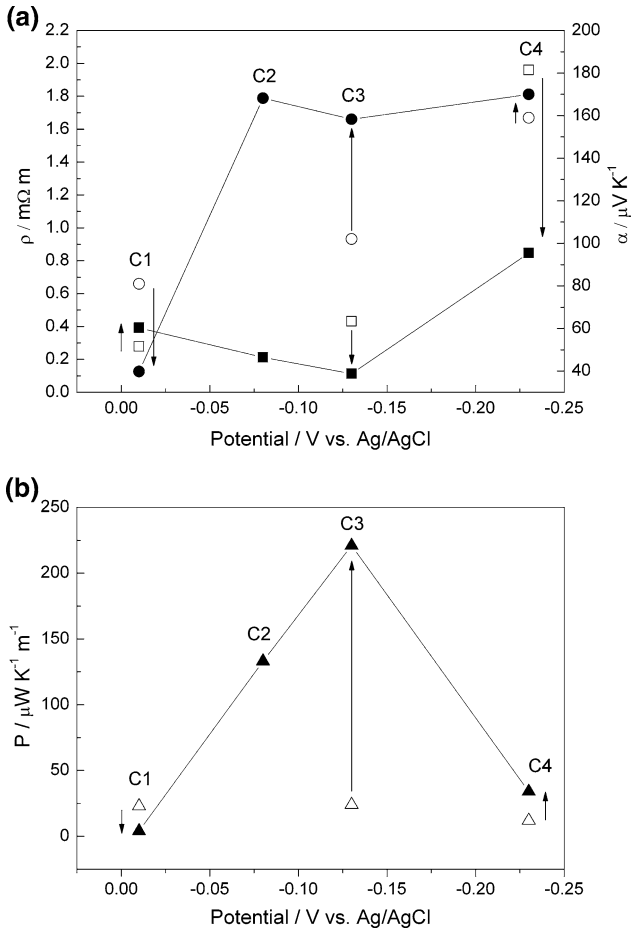

Fig. 4. (a) Electrical resistivity (ρ, square symbols, left y-axis) and Seebeck coefficient (α, round symbols, right y-axis); (b) power factor, $P = \alpha^2\rho^{-1}$, as a function of deposition potential for different $(Bi_xSb_{1-x})_2Te_3$ thin films C1–C4. Arrows indicate changes between values for as-deposited (hollow symbols) and annealed (solid symbols) samples.

Figure 6 shows x-ray diffractograms of the $Bi_2(Te_{1-y}Se_y)_3$ films electrodeposited at different potentials on gold-coated silicon substrates. All diffraction peaks from films E1–E4 are indexed to the rhombohedral space group for the Bi_2Te_3 crystalline type, which indicates that a single phase formed in each film. The peaks appear shifted to smaller d-spacing compared with Bi_2Te_3 and fall in the middle of those observed for $Bi_2Te_{2.7}Se_{0.3}$(PDF 00-050-0954) and $Bi_2Te_{2.5}Se_{0.5}$(PDF 00-051-0643). It is commonly observed that thick films prepared by electrodeposition exhibit strong preferred orientation along (110) planes. However, this is not the case for films E1 to E4 with limited thickness (ca. 0.4 μm), which instead show preferred orientation along (015) planes. For film E1 which contains slightly more selenium than films E2, E3, and E4, the x-ray diffraction peaks (101), (110), (116), (205), and (0210) are not as intense as for films E2, E3, and E4. These differences in relative intensity of

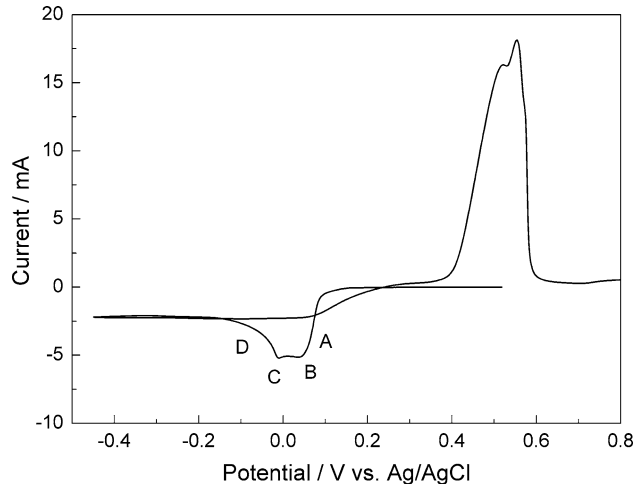

Fig. 5. Cyclic voltammogram of a 1 M HNO_3 solution containing 7.5 mM Bi^{3+}, 1.1 mM SeO_3^{2-}, and 10.0 mM $HTeO_2^+$. The scan starts at the open-circuit potential and proceeds to −0.45 V and is then reversed and swept to 0.8 V using a sweep rate of 10 mV/s. The working electrode is a gold-coated silicon substrate with active area of 0.95 cm^2.

Table II. Dependence of the deposition potential on the elemental composition (atomic percentage) of the prepared film

		As-Deposited (at.%)			
Sample	**E_p (V)**	**Bi**	**Te**	**Se**	**Formula**
E1	0.075	35.9	56.3	7.7	$Bi_{1.8}Te_{2.8}Se_{0.4}$
E2	0.045	37.0	56.1	6.9	$Bi_{1.9}Te_{2.8}Se_{0.3}$
E3	−0.01	37.2	55.8	7.0	$Bi_{1.9}Te_{2.8}Se_{0.3}$
E4	−0.045	37.4	56.0	6.6	$Bi_{1.9}Te_{2.8}Se_{0.3}$

All films were deposited at constant potentials, E_p

the diffraction peaks may reflect different film morphologies, which may in turn affect the thermoelectric properties of the films.

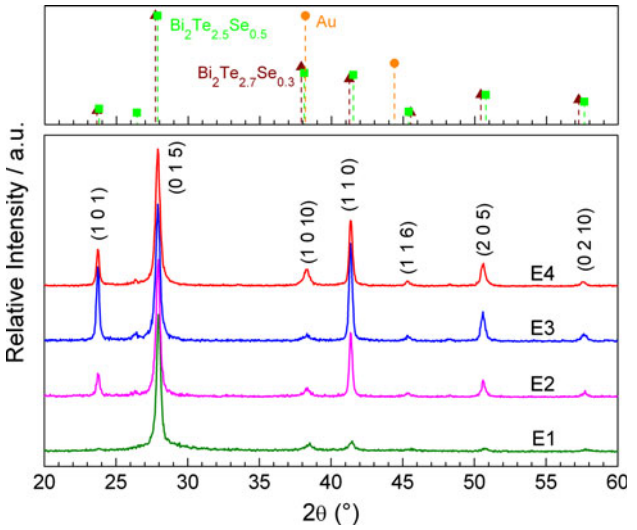

Fig. 6. XRD patterns of as-deposited $Bi_2(Te_{1-y}Se_y)_3$ films prepared at different deposition potentials described in Table II. Intensity is normalized as $(I/I_{max})/\%$, where I_{max} corresponds to the (015) peak. Standard diffraction patterns of gold (dots), $Bi_2Te_{2.7}Se_{0.3}$ (triangles), and $Bi_2Te_{2.5}Se_{0.5}$ (squares) are shown on top.

The differences in surface morphology of films E1 to E4 are shown in the SEM micrographs presented in Fig. 7. The morphology of film E1 features a smooth surface on top of which many discrete needle-shaped clusters are distributed, while films E2 and E3 exhibit a knit-like morphology densely covered by small crystals. The crystallite size becomes smaller in film E4 when the deposition potential is most negative, and the crystal shape resembles that of binary Bi_2Te_3.[23] It has been commonly observed that the surface morphology of the deposited films is not only sensitive to the deposition potential due to the slight change in composition but also sensitive to the substrate that is used; for instance, a nodule-shaped morphology has been found for $Bi_2(Te_{1-y}Se_y)_3$ films eletrodeposited on stainless-steel substrates.[22]

Thermoelectric Properties of $Bi_2(Te_{1-y}Se_y)_3$ Thin Films

Measurements of electrical resistivity and Seebeck coefficient were carried out at room temperature on the as-deposited films after transfer to an insulating epoxy support. Annealing was not performed since all the as-deposited films were highly crystalline as evidenced by the sharp diffraction peaks. Relatively low electrical resistivity compared with as-deposited $(Bi_xSb_{1-x})_2Te_3$ films was found for

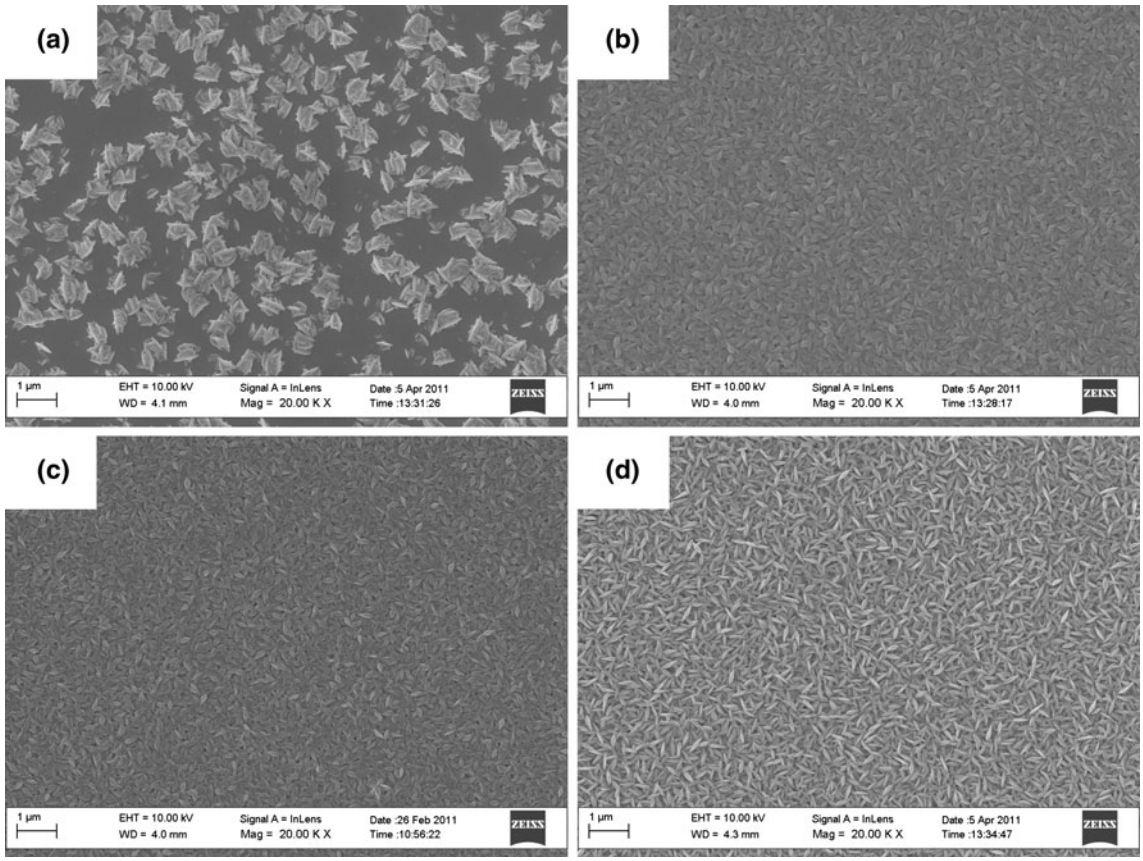

Fig. 7. SEM images of as-deposited $Bi_2(Te_{1-y}Se_y)_3$ films (a) E1, (b) E2, (c) E3, and (d) E4.

different $Bi_2(Te_{1-y}Se_y)_3$ films as summarized in Fig. 8a. The measured values of the Seebeck coefficient are also presented in the same figure. The negative Seebeck coefficient indicates that all deposited films exhibit *n*-type semiconducting features, but the absolute values are consistently lower than that reported (−208 μV/K) for bulk $Bi_2Te_{2.7}Se_{0.3}$.[1] Film E1 showed the highest values of both electrical resistivity and absolute Seebeck coefficient. Decrease in absolute Seebeck coefficient and electrical resistivity was found in films E2, E3, and E4, most likely due to their low selenium content. These Seebeck values are very close to the ones we obtained for electrodeposited *n*-type Bi_2Te_3 films reported previously.[23] In that study we found that the low Seebeck coefficient could be attributed to the high carrier concentration in the electrodeposited films which may result from impurities, nonstoichiometry, and the high density of grain boundaries in the films. Moreover, the electron mobility in the electrodeposited films is considerably low, presumably due to the presence of large concentration of grain boundaries and defects. These imperfections in the films may overshadow the expected effects of selenium substitution for tellurium, which have been suggested to increase the magnitude of the Seebeck coefficient in bulk materials.

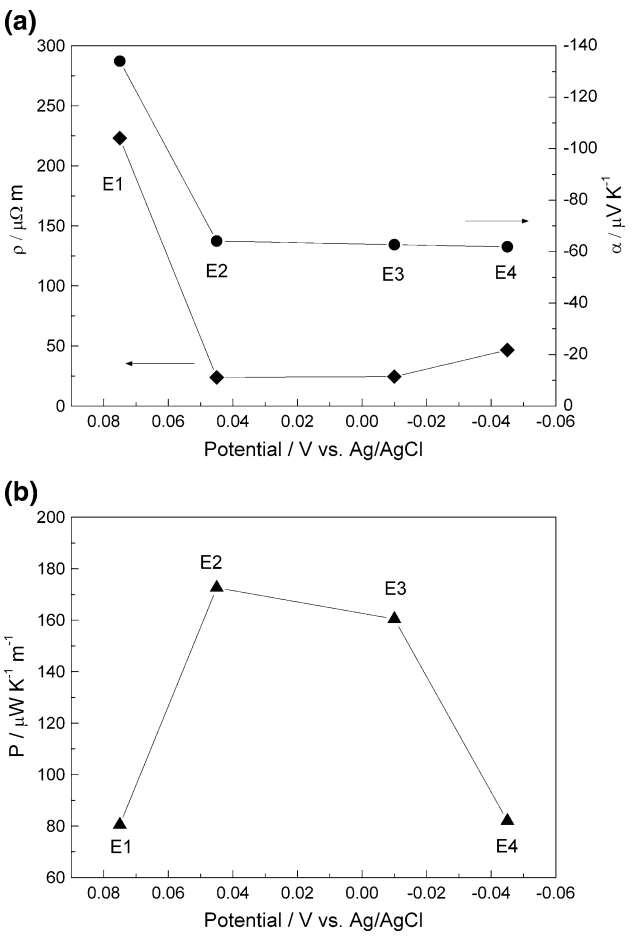

Fig. 8. (a) Electrical resistivity (ρ, diamond symbols, left *y*-axis) and Seebeck coefficient (α, round symbols, right *y*-axis); (b) power factor, $P = \alpha^2\rho^{-1}$, as a function of deposition potential for different $Bi_2(Te_{1-y}Se_y)_3$ thin films E1–E4.

CONCLUSIONS

Thermoelectric thin films of $(Bi_xSb_{1-x})_2Te_3$ and $Bi_2(Te_{1-y}Se_y)_3$ were prepared by electrochemical deposition on gold-coated silicon substrates. The crystal structure, surface morphology, and elemental composition of the films were investigated and correlated to the measured Seebeck coefficient and electrical resistivity. It was found that electrodeposited $(Bi_xSb_{1-x})_2Te_3$ films are *p*-type semiconductors. Near-optimal elemental composition of $Bi_{0.5}Sb_{1.5}Te_3$ can be obtained by depositing at relatively large negative potentials. However, the rough surface morphology and low crystallinity, which requires annealing to improve the thermoelectric properties, may complicate electrochemical preparation of *p*-type multilayer structures based on $Bi_{0.5}Sb_{1.5}Te_3$ and Sb_2Te_3. In contrast, electrodeposited $Bi_2(Te_{1-y}Se_y)_3$ films display *n*-type semiconductivity, and near-optimal elemental composition of $Bi_2Te_{2.7}Se_{0.3}$ can be obtained at relative small negative potentials. The as-deposited films are highly crystalline with thermoelectric properties similar to electrodeposited Bi_2Te_3 films. Therefore, $Bi_2(Te_{1-y}Se_y)_3$ films can be a good candidate for preparation of *n*-type multilayers along with Bi_2Te_3 if a smooth enough surface can be achieved.

ACKNOWLEDGEMENT

The Swedish Foundation for Strategic Environmental Research (Mistra) is gratefully acknowledged for financial support through the E4 Mistra program. A.E.C.P. thanks the Swedish Research Council for support through a Senior Researcher position. The nanofabrication lab (MC2) at Chalmers University of Technology is gratefully acknowledged for assistance with preparation of working electrodes.

REFERENCES

1. G.S. Nolas, J. Sharp, and H.J. Goldsmid, *Thermoelectrics: Basic Principles and New Materials Developments*, Chap. 5 (New York: Springer, 2001).
2. J.P. Fleurial, G.J. Snyder, J.A. Herman, M. Smart, P. Shakkottai, P.H. Giauque, and M.A. Nicolet, *34th Intersociety Energy Conversion Engineering Conference Proceeding, Vancouver*, 992569 (1999).
3. N.K. Abrikosov, T.E. Svechnikova, and S.N. Chizhevskaya, *Neorg. Mater.* 14, 43 (1978).
4. T.C. Harman, B. Paris, S.E. Miller, and H.L. Goering, *J. Phys. Chem. Solids* 2, 181 (1957).
5. H.J. Goldsmid, *Introduction to Thermoelectricity,* Chap. 7 (Springer Series in Materials Science Vol. 121, 2009).
6. R. Venkatasubramanian, E. Siivola, T. Colpitts, and B. O'Quinn, *Nature* 413, 597 (2001).
7. H. Zou, D.M. Rowe, and G. Min, *J. Cryst. Growth* 222, 82 (2001).
8. A. Boulouz, S. Chakraborty, A. Giani, F.P. Delannoy, A. Boyer, and J. Schumann, *J. Appl. Phys.* 89, 5009 (2001).
9. C. Boulanger, *J. Electron. Mater.* 39, 1818 (2009).

10. F. Xiao, C. Hangarter, B. Yoo, Y. Rheem, K. Lee, and N.V. Myung, *Electrochim. Acta* 53, 8103 (2008).
11. Y.T. Miyazaki and T. Kajitani, *J. Cryst. Growth* 229, 542 (2001).
12. M.S. Martin-Gonzalez, A.L. Prieto, R. Gronsky, T. Sands, and A.M. Stacy, *J. Electrochem. Soc.* 149, C546 (2002).
13. B.Y. Yoo, C.K. Huang, J.R. Lim, J. Herman, M.A. Ryan, J.P. Fleurial, and N.V. Myung, *Electrochim. Acta* 50, 4371 (2005).
14. S. Wen, R.R. Corderman, F. Seker, A. Zhang, L. Denault, and M.L. Blohm, *J. Electrochem. Soc.* 153, C595 (2006).
15. G. Leimkühler, I. Kerkamm, and R.R. Koch, *J. Electrochem. Soc.* 149, C474 (2002).
16. Q. Huang, A.J. Kellock, and S. Raoux, *J. Electrochem. Soc.* 155, D104 (2008).
17. V. Richoux, S. Giliberto, and C. Boulanger, *J. Electron. Mater.* 39, 1914 (2010).
18. Q. Huang, W. Wang, F. Jia, and Z. Zhang, *J. Univ. Mater. Sci. Technol. Beijing* 13, 277 (2006).
19. F.H. Li, Q.H. Huang, and W. Wang, *Electrochim. Acta* 54, 3745 (2009).
20. S. Michel, N. Stein, M. Schneider, C. Boulanger, and J.M. Lecuire, *J. Appl. Electrochem.* 33, 23 (2003).
21. L. Bu, W. Wang, and H. Wang, *Appl. Surf. Sci.* 253, 3360 (2007).
22. S. Michel, D. Diliberto, N. Stein, B. Bolle, and C. Boulanger, *J. Solid State Electrochem.* 12, 95 (2008).
23. Y. Ma, E. Ahlberg, Y. Sun, B.B. Iversen, and A.E.C. Palmqvist, submitted for publication.
24. Y. Ma, E. Ahlberg, Y. Sun, B.B. Iverson, and A.E.C. Palmqvist, *Electrochim. Acta* 56, 4216 (2011).
25. W. Zhu, J.Y. Yang, D.X. Zhou, S.Q. Bao, X.A. Fan, and X.K. Duan, *Electrochim. Acta* 52, 3660 (2007).
26. F.H. Li and W. Wang, *J. Appl. Electrochem.* 40, 2005 (2010).
27. L. Qiu, J. Zhou, X. Cheng, and R. Ahuja, *J. Phys. Chem. Solids* 71, 1131 (2010).
28. M.M. Gonzalez, G.J. Snyder, A.L. Prieto, R. Gronsky, T. Sands, and A.M. Stacy, *Nano Lett.* 3, 973 (2003).
29. A. J. Bard, *Encyclopedia of Electrochemistry of the Elements* (New York Cop., 1973–1984).